HAL
open science

Numerical analysis of shear stiffness of an entangled cross-linked fibrous material

Fadhel Chatti, Christophe Bouvet, Guilhem Michon, Dominique Poquillon

To cite this version:

Fadhel Chatti, Christophe Bouvet, Guilhem Michon, Dominique Poquillon. Numerical analysis of shear stiffness of an entangled cross-linked fibrous material. International Journal of Solids and Structures, 2020, 184, pp.221-232. 10.1016/j.ijsolstr.2018.12.001 . hal-02430768

HAL Id: hal-02430768

https://hal.science/hal-02430768v1

Submitted on 7 Jan 2020

HAL is a multi-disciplinary open access archive for the deposit and dissemination of scientific research documents, whether they are published or not. The documents may come from teaching and research institutions in France or abroad, or from public or private research centers.

L'archive ouverte pluridisciplinaire **HAL**, est destinée au dépôt et à la diffusion de documents scientifiques de niveau recherche, publiés ou non, émanant des établissements d'enseignement et de recherche français ou étrangers, des laboratoires publics ou privés.

Open Archive Toulouse Archive Ouverte (OATAO)

OATAO is an open access repository that collects the work of some Toulouse researchers and makes it freely available over the web where possible.

This is an author's version published in: https://oatao.univ-toulouse.fr/21848

Official URL: https://doi.org/10.1016/j.ijsolstr.2018.12.001

To cite this version :

Chatti, Fadhel and Bouvet, Christophe and Michon, Guilhem and Poquillon, Dominique Numerical analysis of shear stiffness of an entangled cross-linked fibrous material. (2020) International Journal of Solids and Structures, 184. 221-232. ISSN 0020-7683

Any correspondence concerning this service should be sent to the repository administrator:
tech-oatao@listes-diff.inp-toulouse.fr

Numerical analysis of shear stiffness of an entangled cross-linked fibrous material

Fadhel Chatti[a], Christophe Bouvet[a], Guilhem Michon[a], Dominique Poquillon[b,*]

[a] Institut Clément Ader, CNRS UMR 5312, Université de Toulouse, ISAE-SUPAERO, 3 Rue Caroline Aigle, Toulouse 31400, France
[b] CIRIMAT, Université de Toulouse, INP-ENSIACET, 4, allée Emile Monso, BP 44362, Toulouse Cedex 4, Toulouse 31432, France

Keywords:
Entangled cross-linked fibres
Finite element model
Shear stiffness

A B S T R A C T

The objective of this paper is to understand and study the effect of morphological parameters on the shear stiffness of an entangled cross-linked fibrous material made with carbon fibres where some of the contacts are bonded by the epoxy resin. This current work presents a 3D finite element model using ABAQUS/Standard in order to characterize the mechanical behaviour of different carbon fibre networks rigidified by epoxy cross-links. Numerical simulations are achieved on a representative volume element (RVE) with the orientation distribution of the fibres based on a tested sample. Since not all the strands are perfectly separated, an equivalent diameter of fibre is determined to obtain the rigidity experimentally measured in shear. Then, an investigation of the influence of morphological descriptors, such as the distance between cross-links, distribution fibre orientations and junction properties, is carried out. For the entangled cross-linked fibrous material with a small fibre volume fraction, the relationship between the shear stiffness and the fibre volume fraction is a linear function whereas the relation between the shear stiffness and the distance between junctions is a power law with exponent of −3/2. The shear stiffness depends slightly on the twisting joint stiffness, and its relationship with the tension joint stiffness is a logarithmic function. The effect of fibre stiffness is also investigated by taking Young's modulus values corresponding to those of glass fibres, inox fibres or aramid fibres. A linear function is obtained between the shear stiffness and the Young's modulus. These results are consistent with the analytical models in the literature for a cross-linked fibrous material.

1. Introduction

Composites are increasingly used in industrial applications and especially in the aerospace field due to their attractive stiffness to weight ratios (Castanié et al., 2008; Belouettar et al., 2009). The sandwich structure occupies an important place in the manufacturing of composite parts. Its composition of two rigid skins spaced by a light core of great thickness and low stiffness offers a high stiffness for bending applications. Numerous core materials with different configurations have been designed and studied in the literature (Mezeix et al., 2009). The honeycomb is still the most used core material for the sandwich structure because it offers the best stiffness to weight ratio. However, it presents many drawbacks, such as the difficulty implementing it in complex structures, closed porosity and difficult quality control processes. The low vibration damping is still the most important problem with the honeycomb structure, and many methods have been presented to enhance the damping of the sandwich structure (Cai et al., 2004; Fotsing et al., 2013; Li, 2006).

Based on the study of Poquillon et al. (2005), Mezeix et al. (2009),(2015a) developed a new entangled cross-linked material that can offer good vibration damping (Piollet et al., 2016) due to the energy dissipated through friction between fibres. The honeycomb cannot yet be substituted by this new material in the aerospace field because its shear stiffness is very low. The numerical modelling of the entangled cross-linked material seems necessary to understand and study its behaviour. Whereas the honeycomb has been significantly studied in the literature (Silva and Gibson, 1997; Kallmes and Corte, 1960), only a few investigations have been conducted to study such fibrous materials.

The creation of models aimed at enhancing the understanding of the mechanical behaviour of fibre assemblies started with analytical models (Gibson and Ashby, 1997; van Wyk, 1946). Although the previous analytical models were confined to rather simple uniform arrays, they provide data of great interest. In 1952, Cox (Cox, 1952) proposed an analytical model in which the fibres

* Corresponding author.
E-mail addresses: fadhel.chatti@isae.fr (F. Chatti), christophe.bouvet@isae.fr (C. Bouvet), guilhem.michon@isae.fr (G. Michon), dominique.poquillon@ensiacet.fr (D. Poquillon).

https://doi.org/10.1016/j.ijsolstr.2018.12.001

were not supposed to interact with each other, extend from one edge of the network to the other and transmit only an axial load. His model derived the elastic coefficients as a function of the fibre orientation distribution. According to Cox's studies and for a three-dimensional isotropic assembly, the results are:

$$\text{The elastic modulus}: \ E = \frac{k}{6} \tag{1}$$

$$\text{The shear modulus}: \ G = \frac{k}{15} \tag{2}$$

where $k = \frac{\rho_s}{\rho_f} E_f$

and ρ_s, ρ_f and E_f denote the fibrous material density, the density of the fibre and the elastic modulus of fibre, respectively. The predicted stiffness values could be viewed as an upper limit that cannot be reached in real fibre networks.

Van den Akker (1962) assumed that the non-bonded parts of the fibres can also support shear and bending, apart from axial strain. He considered the bonds to be rigid and to rotate to an extent equal to the mean of the rotations of the two cross-linked fibres. He concluded that two groups of stress cause rupture of fibre-to-fibre bonds: those associated with tension in the fibres and those associated with torque on the bonds due to the shear force in the fibre segments.

In 1960, Kallmes and Corte (1960) presented a model dealing with the morphology of fibre networks. Their model was applied to the study of paper. The authors assumed that the fibres were independently deposited of each other and the fibre network had a uniform orientation distribution. They stated that the geometric arrangement of the fibres was an effect of the paper making process and the cause of the paper's properties. The relationships between the paper properties and the different morphological properties of the assembly, such as the average length of the straight segments between contacts, the number of fibre crossings, the fibre volume fraction and the elastic properties of the fibres, were presented. Among its results, the following equation established the average number of fibres crossings in a square of side length, L:

$$n_c = \frac{\left(n_f l_f\right)^2 c^2}{L^2 \pi} \tag{3}$$

where n_f is the number of fibres, l_f is the average length between contacts and c denotes the average curl index, which is the distance between the fibre end points divided by the fibre length.

Another equation from Kallmes and Corte provides the average length l_s of free segment without contact on a fibre:

$$l_s = \frac{n_f l_f c}{2 n_c} \tag{4}$$

Kallmes et al. (1963) proposed an investigation based on the calculations of Van den Akker (1962) that emphasized the effect of the free and bonded parts of the fibre segments.

Eqs. (3) and (4) have been presented for 3D fibre networks by Komori and Makishima (1977). Their theories used curved beams and considered the influence of curliness, fibre sliding and crimp. Although their model qualitatively presents the behaviour of fibre assembly, its applicability is limited because it assumes affine deformation of the inter-fibre contact points.

The fibre network made by inducing cross-links at the fibre contact can be considered to be a particular kind of foam-like material. Thus, the Ashby and Gibson's methods, concerned with the modelling of open cellular solids (Gibson and Ashby, 1997b; Ashby et al., 2000), can be used for the fibre cross-linked assembly. The authors model is based on beam deflections. Ashby and Gibson proposed an expression calculating the compression modulus of open cell foam:

$$E = \frac{3\pi E_f}{4\left(\frac{L}{D}\right)^4} \tag{5}$$

where E_f is the Young's modulus of fibre, L is the distance between joints and D is the fibre diameter.

Heyden (2000) developed a finite element model for the geometrical linear deformation of cellulose fibre assemblies with an isotropic orientation distribution. The fibres were modelled by beam elements with a constant curvature and introduced in a periodic representative volume. The fibre contacts were represented by a set of springs that allowed stick-slip. They were bonded in the sense that once created, the springs cannot be broken. The model provided simulation results that were in good agreement with experiment results. However, it was tested only for low fibre volume fraction, $f = 3\%$.

Delince and Delannay (2004) developed an analytical model that was based on a periodic network architecture to determine the elastic properties of transverse isotropic steel fibre arrays. The Young's moduli calculated from their model were below experimental values. They assumed that this difference was due to the negligence of triangulation effects in the model. Delannay (2005) proposed a new model that accounts for the negative Poisson ratio behaviour and the random triangulation. His model predicted the shear stiffness, G_{13}, properly. However, no such agreement was verified for the predictions of the in-plane modulus, E_1, and the out-of-plane modulus, E_3, which were notably lower than the measured values. Even if the model did not provide a full quantitative agreement with the experiment results, it can offer indications for optimizing the design of the fibre orientation distribution that can give the most suitable elastic anisotropy for the aimed application. It follows that the predictions of the new model for the in-plane shear modulus, G_{13}, appeared to agree with the value measured for the reference material.

A simple analytical model was developed by Markaki and Clyne (2005) to predict the mechanical behaviour of non-periodic bonded fibre assemblies when subjected to either magnetic or mechanical loads. This model assumed that the bending of the individual fibres dominated the deformation. None of the changes in morphology during compression was taken into account. Only the initial geometry of the material was considered. It can therefore be applied only to cases in which the fibre segments between the bonds are slender ($L/D \geq 3$). An expression was derived for the Young's modulus, and it is similar to that of the Gibson and Ashby's model (Gibson and Ashby, 1997b; Ashby et al., 2000) that is based on a regular and orthogonal set of fibres, except that the fibre segment aspect ratio, L/D, and the fibre volume fraction, f, can be independently specified. Compared with experiment, the results provided by this model were limited due to the difficulties in reliably estimating L/D.

Mezeix et al. (2015b) developed an analytical model to investigate the behaviour of entangled cross-linked fibres under a tensile and compressive load. Like the Markaki and Clyne (2005), the form of their prediction was based on the fibres bending. However, the cross-links (epoxy joints) were modelled by twisting springs that were applied at the extremity of the beam. This model considered the additional rigidity in tension due to the quasi-vertical fibres that made the stiffness in tension higher than the one in compression. The quasi-vertical fibres were considered to buckle quickly during the compression test.

Recently, a 3D periodic beam model was proposed by Ma et al. (2018) to investigate the elasto-plastic characteristics of porous metal fibre sintered sheets (MFSSs). The establishment of the finite element model was carried out progressively with the

2D coordinates considered first. By piling up the fibres one by one until N fibres were layered in the model, the growth in the out-of-plane dimension was considered. At the fibre intersections, additional beam elements were inserted to model the cross-linkers whose density had a significant role in both the strength and the stiffness of the stochastic fibre network. The simulation results showed good agreement with the dimensional analysis and experimental data (Jin et al., 2013).

In the literature, the previous analytical models, investigating the stiffness of a fibrous material with permanent junctions, do not consider the variations in the morphology of the assembly during mechanical loading. In addition, the compression stiffness of a fibrous material was much more studied than the shear stiffness, which can be more important when the fibrous material is used as a core material in a sandwich structure, such as for the entangled cross-linked fibrous material of the present study.

The objective of this work is to investigate the shear stiffness of an entangled cross-linked fibrous material and the dependence of the shear modulus on the morphological parameters, such as the distance between the junctions, the fibre volume fraction, the joint stiffness and the distribution of the fibre orientations.

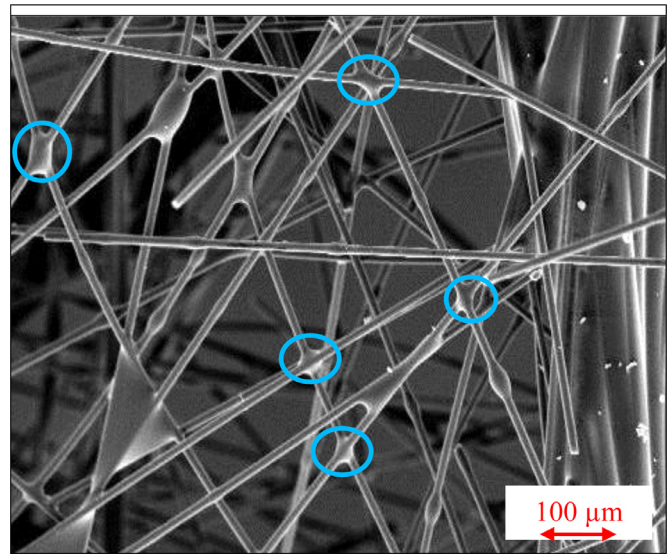

Fig. 1. SEM observation of entangled cross-linked carbon fibres with a volume fraction, f, of 8.5%; The Blue circles indicate some of epoxy cross-links.

2. Simulation methods

An entangled cross-linked material can be made by different types of fibres, such as carbon, glass or aramid (Mezeix et al., 2009, 2015a), that were cross-linked by a thermo-hardening resin. Carbon fibres were mainly used to manufacture the entangled cross-linked material in order to obtain a higher mechanical performance, though its cost is higher. Filament carbon is characterised by a diameter of 7 µm, an elastic modulus of 240 GPa and a bulk density of 1770 kg/m^3. Epoxy was chosen as the resin for cross-linking because it is widely used in aerospace applications. The manufacturing process of these materials was carried out manually at the laboratory scale and has been detailed in previous studies (Mezeix et al., 2009, 2015a). The yarns were cut to a fixed length (12 mm), introduced in a 64 l parallelepiped box in which a compressed air flow (6 bars) was applied to separate the fibres. Separation and entanglement were carried out together. The material thus obtained was exposed to an epoxy spray to obtain attached epoxy droplets in some of contacts between fibres. A given mass of this material was then placed into a mould for the last step of the process: the polymerization of the epoxy resin (8 h into a temperature chamber at 70 °C). The samples were then demoulded. An image of the manufactured material's microstructure is shown in Fig.1.

The numerical modelling was based on experimental tests in which a sample of entangled cross-linked material, with a size of $20 \times 40 \times 60$ mm^3, was solicited in shear (Piollet et al., 2016). The whole sample contained more than three million carbon fibres for a fibre volume fraction of 8.5%. In this case, the numerical modelling of an entire sample would be complicated and incur a high computational cost. Therefore, a representative volume element (RVE) was chosen for the model. Its side dimension was 1 mm, which is the most appropriate choice to guarantee the stability of the morphological parameters (distance between contacts, distribution of fibre orientations) in each draw with a minimum of computational cost (Chatti et al., 2018a). The architecture of the RVE was generated from an in-house pre-processing program coded in FORTRAN and presented in previous work (Chatti et al., 2018a, 2018b).

This numerical modelling considered the initial distribution of fibre orientations that were close to the architecture of the real sample before loading. Indeed, when the fibres were packed in the mould, the entangled fibres lost their initial isotropic distribution, so a transversally isotropic material was obtained after the polymerisation step. Then, a numerical technique was developed to identify the fibre direction distribution after the moulding process. Fig. 2 shows the distribution of fibre orientations (green curve) that was used to represent the architecture of the real sample, and it is compared to the theoretical isotropic fibre distribution (black curve in Fig. 2). In the numerical anisotropic fibre distribution, there are more fibres with directions characterized by an angle θ close to 90°. This angle corresponds to the perpendicular direction to the vertical axis and it describes the quasi-horizontality of fibres after being packaged in the mould. More details of this technique can be found in the previous paper (Chatti et al., 2018b).

The finite element solver in ABAQUS/Standard was used in the actual work to accurately determine the shear stress. It uses technologies that are ideal for the determination of highly accurate stress solutions. Each fibre was modelled by a series of 3D beam elements (ABAQUS element type B31) depending on both the number of intersections between the fibres and on their orientation in the RVE that determined their length in the computation. This element type is based on the Timoshenko beam theory that allows for shear deformation. The strains considered here are of small amplitude, less than 1%. The dominant mode of deformation of the assembly is the bending of the elastic carbon fibres. For this reason, it is the tensile/compressive behaviour of individual fibres in the fibre direction that must be taken into account. Moreover, even if the transverse stiffness of the fibre is different of the longitudinal one, this transverse behaviour does not affect the bending stiffness of fibre. Then, based on previous work (Piollet et al., 2016; Chatti et al., 2018a), the behaviour of the fibres has been simplified and each fibre is assumed to have an isotropic linear elastic behaviour. Springs were introduced in the model through the user element to model the epoxy cross-link. In the previous paper (Chatti et al., 2018a), a finite element model of two fibres that were bonded by epoxy junction was used to determine the stiffness that should be introduced in the spring and can describe the behaviour of the epoxy junction. The material properties of the epoxy cross-links were assumed to be an isotropic linear material with Young's modulus $E = 5$ GPa and Poisson ratio $\nu = 0.3$. At the end of the numerical investigation, two stiffnesses were determined. The tension stiffness, K_{te}, was equal to 0.4 N/mm, while the twisting stiffness, K_{tw}, was equal to 3.10^{-4} N.mm (Chatti et al., 2018a). Each simulation used four parallel processors and 12 GB of memory in total, and it lasted a few minutes. A few thousand carbon fibres were

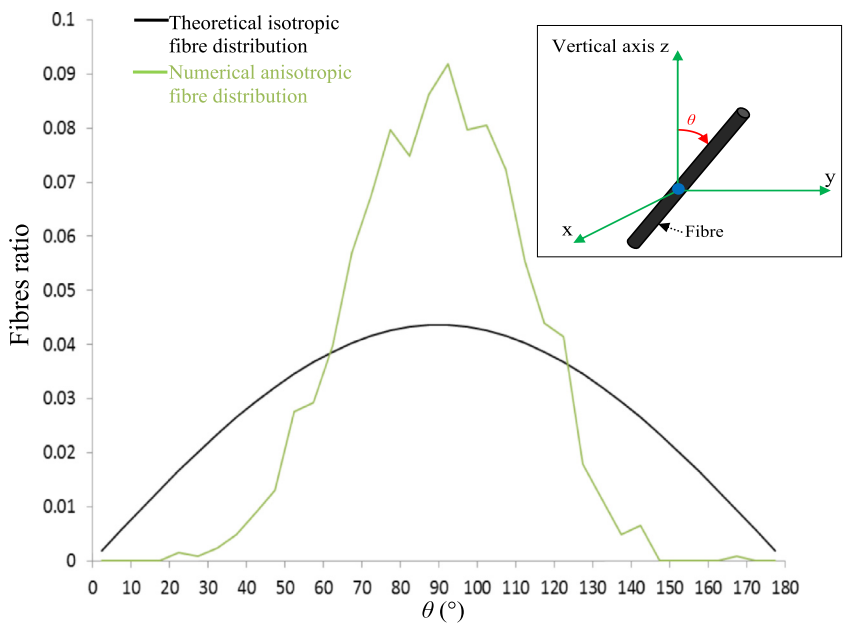

Fig. 2. Different fibre orientation distributions. The solid black curve (sinus) represents the theoretical distribution obtained in the case of a perfectly random orientation of the fibres in 3D, i.e. an isotropic distribution of the fibre assembly. The solid green curve represents the anisotropic distribution that is closer to the experimental sample (Chatti et al., 2018b). The angle θ is the angle between the fibre direction and the vertical axis, z.

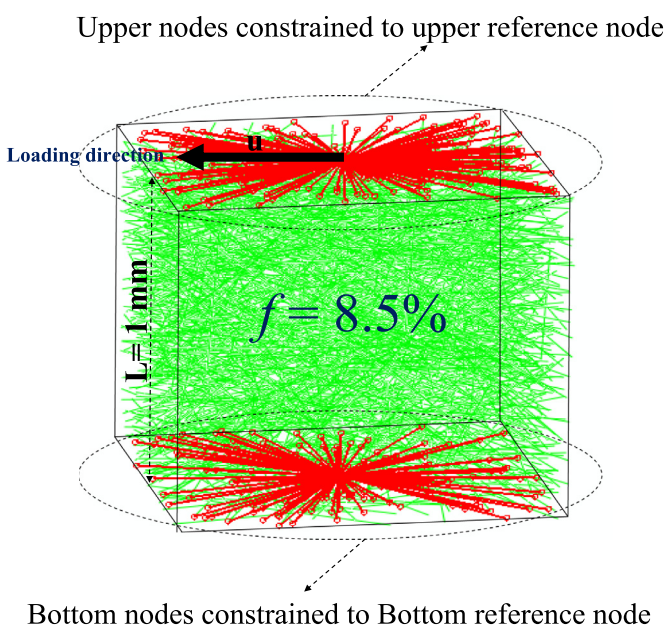

Fig. 3. Three-dimensional view of the RVE with the size of $1 \times 1 \times 1$ mm^3. Kinematic coupling, of the nodes of the upper and bottom face with two reference nodes, were used to apply the shear load.

generated inside the cubic RVE with a size of $1 \times 1 \times 1$ mm^3 in order to reach a targeted initial volume fraction of 8.5%.

In the experimental tests, 3 mm-thick aluminium plates were glued on each side of the entangled cross-linked sample (Piollet et al., 2016) while the other faces were free. To apply the boundary conditions that respected the general conditions of the experimental test, the nodes for the upper and bottom faces of the RVE were constrained to the upper reference node and bottom reference node, respectively, as illustrated in Fig. 3. These two reference nodes governed the motion of the nodes for the upper and bottom faces. In order to apply the shear load, the upper one moved to the left while no motion was allowed for the bottom one. The shear strain applied to the upper reference node was equal to 1% so that the expression of the shear strain was $\gamma = u/L$. All the other nodes were free to move.

The ABAQUS/Standard (User Documentation) cannot manage the interaction between pairs of fibres and the interaction of one fibre with itself. Indeed, this commercial software basing on implicit schema of integration cannot detect the surface of contact between the intermediate parts of beam elements; it just allows the interaction between the extremities of beam elements. However, the other software "ABAQUS/Explicit" (User Documentation) is more appropriate for the management of different contacts but we did not use it in this actual work because the objective was to obtain faster results for the linear part of the behaviour of the entangled cross-linked fibre material, which corresponds to small deformations and during which the morphology of the assembly changes little as does the number of contacts (Piollet et al., 2016; Gibson and Ashby, 1997b; Markaki and Clyne, 2005; Chatti et al., 2018a). So, ABAQUS/Standard is the best candidate in this case, when the rigidity of entangled cross-linked material is mainly due to the fibre network and to the epoxy bonds (Mezeix et al., 2009).

The total time period used in the loading step was equal to 1 s. It is a fictive time that does not impact the elastic linear calculation. The initial time increment chosen was 0.1 s. The time increment allowed was between 1 µs and 0.1 s.

3. Results and discussion

3.1. Shear test

First, the $1 \times 1 \times 1$ mm^3 cubic RVE, that contained 2430 carbon fibres with a diameter of 7 µm and Young's modulus of 240 GPa, was solicited in shear. The initial volume fraction was 8.5%. The numerical fibre diameter corresponded to the real carbon fibre, which was equal to 7 µm. Thus, a numerical case of perfect yarn separation was treated. The anisotropic fibre orientation (Fig. 2) was generated in this RVE following the previous data. This mix of morphological parameters provided around 25,000 contacts between the fibres and more than 60,000 beam elements. The technique used to block the contacts (thus positioning the springs)

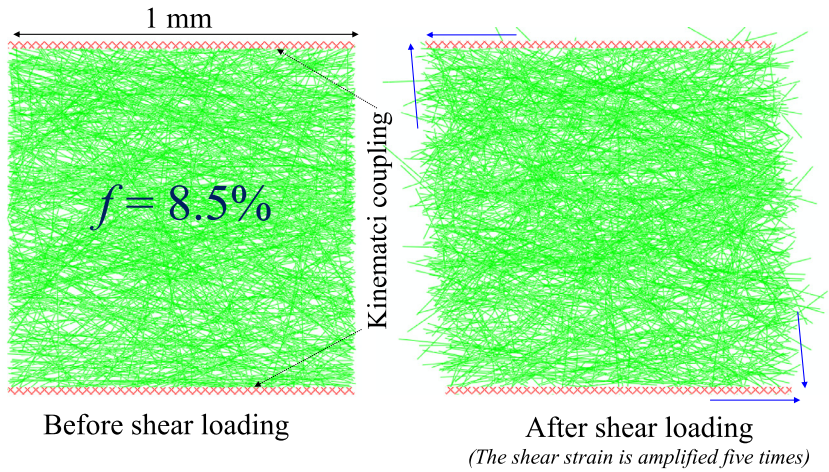

Fig. 4. The view in front of the RVE geometry before and after shear loading where $\gamma = 1\%$.

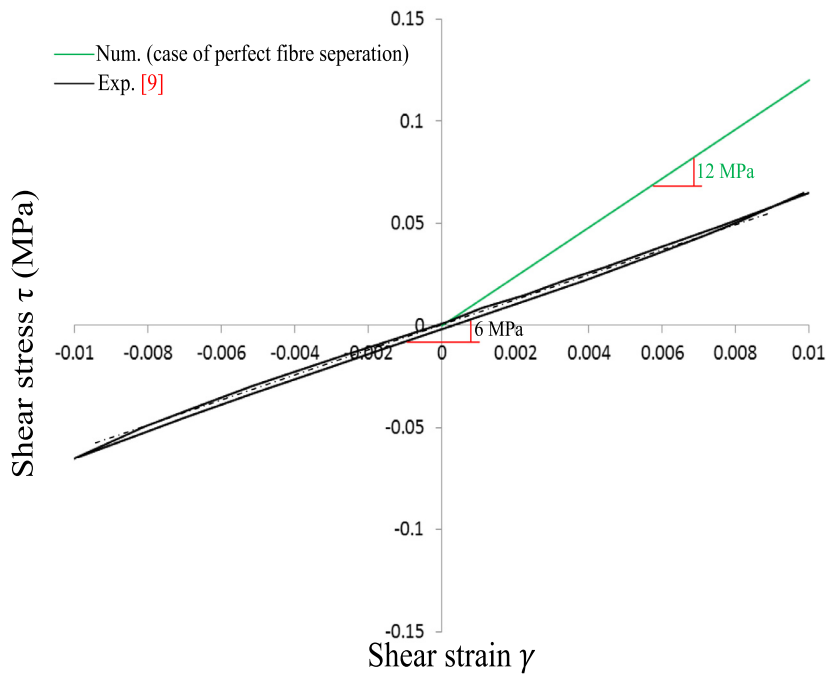

Fig. 5. Comparison between the experimental curve (Piollet et al., 2016) in black and numerical simulation in green for $f = 8.5\%$ and a fibre network with fibre orientation representative of the experimental data. This consisted of perfectly separated strands with a fibre diameter of 7 µm on which two out of three contacts were glued. The black dashed black line corresponds to the value of the linear rigidity of the network identified in (Piollet et al., 2016), where $G = 6$ MPa.

consists in blocking a given proportion of the contacts. This is illustrated in Fig. 9. In the previously described configuration, two thirds of the contacts were bonded with cross-links in the shape of springs in order to get an average distance between the junctions equals to 122 µm. This value is similar to the experimental value of 120^{+140}_{-70} µm estimated experimentally by Mezeix et al. (2015a).

Fig. 5 shows the curve of the shear stress versus the shear strain in the case of a perfect fibre separation. The curve is elastic linear in view of the finite element hypothesis. It is shown with a green line and is steeper than the experimental curve (Piollet et al., 2016). The shear modulus for this case was equal to 12 MPa, which is about two times the value obtained during experimental tests.

This difference can be explained by the yarns that were not well separated during the manufacturing of the entangled cross-linked samples (Fig. 6). The entangled cross-linked material was heterogeneous and all yarns were not perfectly separated after the entanglement step. The modelling of the yarns in the RVE was difficult due to the lack of the necessary data about the size and the position of these yarns in the sample. Due to the small size of the fibre, it was not possible until now to get statistical data for a RVE through the 3D tomography work. Then, the quantity and the size of the remaining yarns were not known enough to get statistical data for modelling the RVE. Furthermore, the developed numerical approach allowed the use of only beams with a homogeneous diameter. It was then complicated to model the non-separated yarns and these remaining yarns are beams of variable diameters (two to ten fibres can be joined together) and of variable stiffness. The assumption made is the following: this distribution can be replaced by having a beam with a diameter greater than the one of a single fibre, whose cross-section and rigidity are equal to that of two adjacent fibres. This equivalence is explained in Fig. 7. A homogeneous fibre with a diameter D_h of $7\sqrt{2}$ µm and Young's modu-

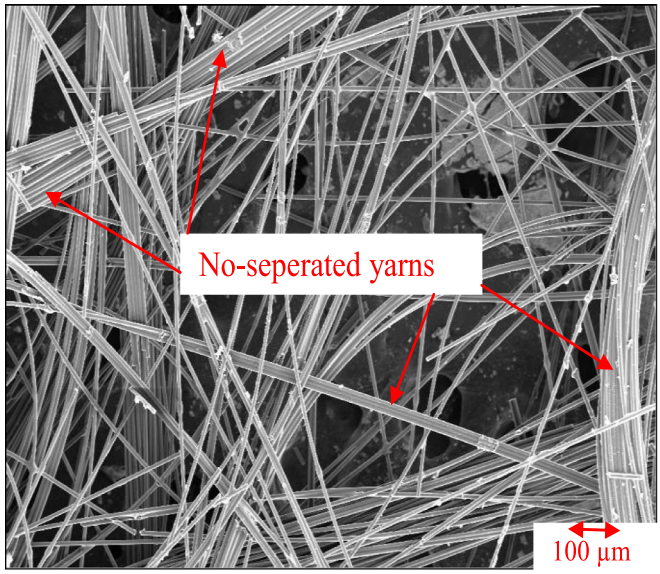

Fig. 6. The SEM observation of an entangled cross-linked material made with carbon fibres of Ø 7 μm; some of the yarns still existed and were heterogeneously dispersed.

lus of $E_h = 120$ GPa, which is the half of that for a real carbon fibre, was used to target a bending stiffness equal to that of one of yarn that is composed of two fibres. This assumption was successfully tested and used to model the hysteresis loop in the previous work (Chatti et al., 2018). As the deformation of the material results mainly from the bending of the beams (Markaki and Clyne, 2005; van Wyk, 1946), the decrease of the axial stiffness of segments by half, has not an important effect on the general results because the stretching can be neglected against the bending deformation (Gibson and Ashby, 1997; Markaki and Clyne, 2005; van Wyk, 1946).

In this new case, 1230 carbon fibres were generated in the RVE to obtain a fibre volume fraction equal to 8.5%. The distribution of fibre orientations is the same than in the previous calculations and induced anisotropy, as illustrated in Fig. 2. The average distance between the junctions was around 160 µm. This average distance was obtained by blocking two out of three contacts (Fig. 9-b). Around 6000 among 9000 contacts were blocked by the springs. This value of 160 µm is comparable to the experimental value of 120^{+140}_{-70} µm reported by Mezeix et al. (2009) but slightly larger.

Fig. 8 shows curve of the shear stress versus shear strain that allowed the evaluation of the shear modulus in the case of non-separated fibres. The comparison between the numerical curve and experimental data indicates a good agreement in terms of shear stiffness. Numerically, the shear modulus value is of the same order of magnitude as the experimental one. It is equal around 7 MPa, whereas the experimental value is about 6 MPa (Silva and Gibson, 1997).

In order to check the repeatability of the results of the numerical simulation, three different geometries were generated. Indeed, in the previous works (Chatti et al., 2018a, 2018b), we have checked the volume chosen for the simulation (a cubic millimetre), was a RVE in the morphological sense (Kanit et al., 2003). It was then important to verify that we had a representative elementary volume for mechanics. Table 1 presents the parameters of each draw and the values of the shear modulus calculated in each case. Numerical values are very close with a small dispersion that can be explained by the dispersion between the draws that were generated. In this small dispersion, the numerical results show that the shear stiffness increased linearly with the fibre volume fraction and it increased non-linearly with the average distance between junctions. These observations agree with the previous studies of fibrous materials.

In the following sections, some morphological parameters will be modified in the geometry of the RVE made with homogeneous fibres in order to study the evolution of the shear modulus. Five parameters will be involved: the fibre volume fraction, the initial distribution of fibre orientations, the average distance between cross-links, the joint tension stiffness and the joint twisting stiffness.

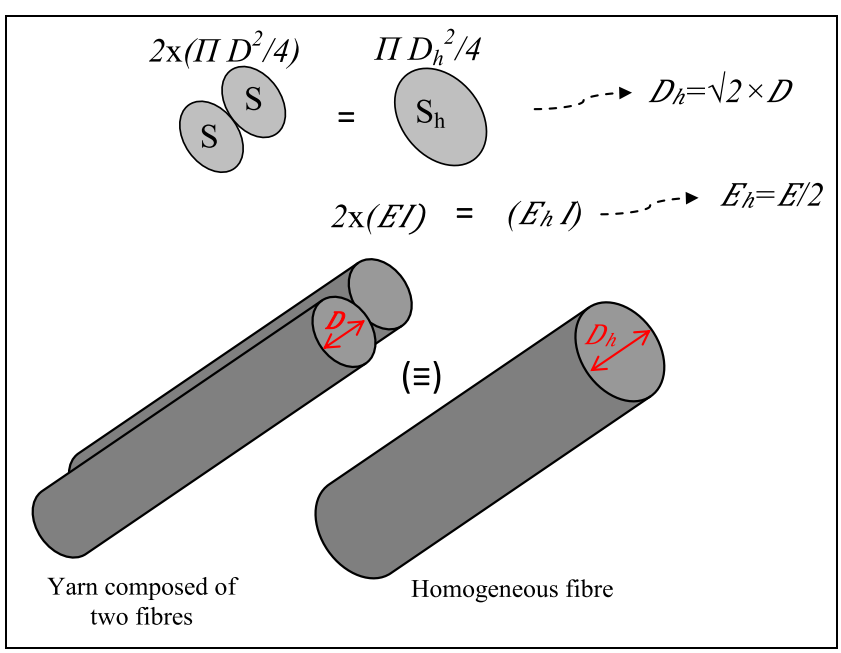

Fig. 7. Technique used to consider the non-separated fibres. A big fibre with a diameter $\boldsymbol{D_h} = 7\sqrt{2}\ \boldsymbol{\mu m}$ is equivalent to two non-separated fibres with a diameter 7 $\boldsymbol{\mu m}$ in terms of bending stiffness.

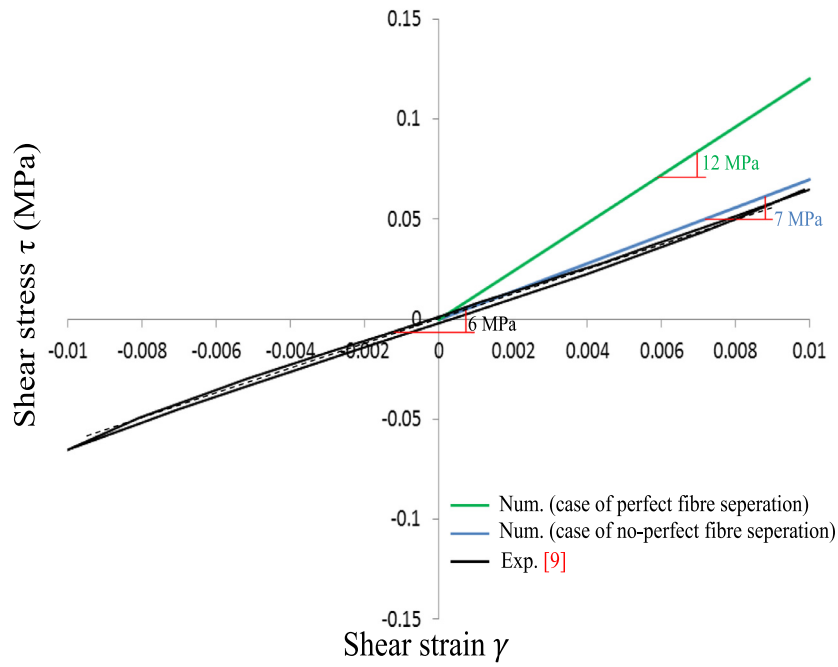

Fig. 8. Comparison between experimental data and numerical results for a fibre volume fraction $f = 8.5\%$. The blue curve corresponds to the simulation using a fibre diameter equal to $\boldsymbol{D_h} = \boldsymbol{D}\sqrt{2} = 7\sqrt{2}$ µm and a Young's modulus $E_h = E/2 = 120$ GPa. The green curve corresponds to the simulation using a fibre diameter equal to $\boldsymbol{D} = 7$ µm and a Young's modulus $E = 240$ GPa (Fig. 7).

Table 1
Details of the three different simulations carried out with three different random draws of the position of the fibres.

	Number of beam elements	Fibre Volume fraction (%)	Number of cross-links	Average distance between non-bonded contacts (µm)	Average distance between cross-links (µm)	Shear modulus G (MPa)
RVE 1	21646	8.58	6115	330	165	7.2
RVE 2	21543	8.45	5952	336	168	6.8
RVE 3	21608	8.51	6082	334	167	7

3.2. Effect of morphological parameters on the shear modulus

3.2.1. Effect of the distance between cross-links on the shear modulus for different distributions of fibre orientations

The distance between the cross-links is considered to be one of the principal parameters related to the stiffness of a fibrous material. It depends on the quantity of pulverized resin and on the fibre volume fraction.

In this paragraph, the influence of the distance between cross-links for different distributions of fibre orientations will be evaluated. The values of other morphological parameters were fixed. The initial fibre volume fraction was equal to 8.5%, the tension stiffness, K_{te}, was equal to 0.4 N/mm while the twisting stiffness, K_{tw}, was equal to 3.10^{-4} N.mm.

In this work, four initial distributions of the fibre orientations were studied, as illustrated in Fig. 10-b. The red colour curve represents the distribution obtained in the case of a random orientation of the fibres in 3D, i.e. an isotropic distribution of the fibre assembly. The three other distributions were anisotropic characterised by more fibres with horizontal directions (the shear loading direction in the Fig. 3). In Fig. 10-a, four curves are plotted and each curve was formed by four points corresponding to the ratio of the bonded contact. The method that was used to perform each ratio is presented in the Fig. 9 (a, b, c and d), which correspond to the four ratios of the bounded contact, namely 1/1, 2/3, 1/2 and 1/3, respectively.

In Fig. 10, four curves present the shear modulus as a function of distance between the cross-links, D_c. When the last one increased, the shear modulus decreased for the four cases. More precisely, for the four assemblies of fibres tested with four different fibre orientation distributions, the results between the shear stiffness G and the distance between junctions D seem to follow a power law $G = a.D^b$ with an exponent $b = -3/2$. This exponent is slightly lower than the one deducted by Markaki and Clyne (2005) (−2). This may be due to our boundary conditions at the level of the junctions which are more flexible than the infinite rigid cross-links in the analytical model of Markaki and Clyne (2005). The shear stiffness increased in the same way, regardless of the distribution of the fibre orientations (Fig. 10-a). Thus, the effect of the distance between the cross-links did not change if the distribution of fibre orientations was isotropic or anisotropic.

The shear modulus clearly depended on the two morphological parameters, namely the distribution of orientation fibres and the distance between cross-links, as illustrated in Fig. 10-a. For the distribution of experimental samples (the green curve), the numerical simulation result provided a shear modulus equal to 16 MPa when each contact between the fibres was bonded.

The high shear modulus value was obtained when the distribution was isotropic and the average distance between cross-links was around 110 µm, which corresponds to the case in which all the contacts between the fibres were glued by epoxy junctions. It can reach more than 50 MPa. This shear modulus value is still smaller than for a Nomex honeycomb, which is equal to about 120 MPa (Zenkert, 1997). However, it is close to the shear modulus of foam PMI 110, which is equal to about 50 MPa.

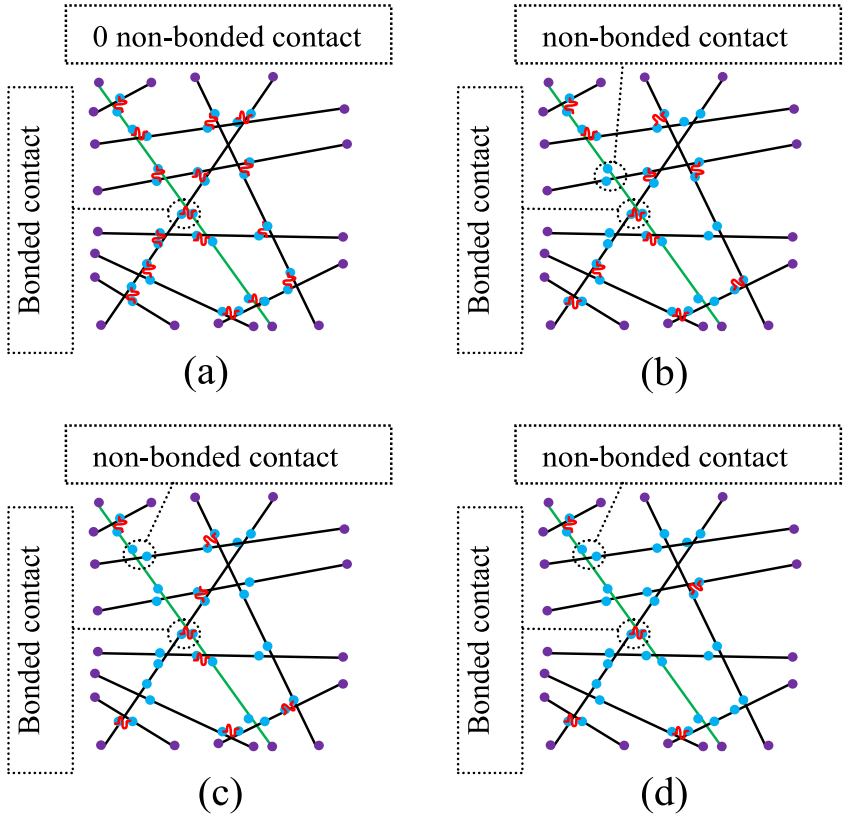

Fig. 9. The way used to generate springs linking the contacts of one fibre, which is coloured in green, to the other fibres. These are illustrations in the case where (a) all contacts were blocked, (b) two out of three contacts were blocked, (c) one out of two contacts was blocked and (d) one out of three contacts was blocked.

The manufacturing of an entangled cross-linked fibrous material in which all contacts would be bonded by epoxy cross-links could increase the stiffness of the material but probably reduce the vibration damping, which is the most important property of the cross-linked material. A compromise between energy dissipation through dry friction and shear stiffness should be considered.

3.2.2. Effect of the distance between cross-links and fibre volume fraction on the shear modulus

In this section, the influence of the distance between the cross-links on the shear stiffness was evaluated for different fibre volume fractions. Maintaining the same size of the RVE as $1 \times 1 \times 1$ mm^3 and the same distribution of fibre orientations (Fig. 2), the variation of the fibre volume fraction was followed necessarily by a variation in the number of contacts and a subsequent variation in the distance between junctions. As in the previous section, four ratios of bonded contact were studied: 1/1, 2/3, 1/2, and 1/3. The effect of the distance between the cross-links on the shear modulus for different fibre volume fractions is shown in Fig. 11-a. Three different initial fibre volume fractions were tested. The smaller fibre volume fraction, which was tested, was equal to 6.5%. As checked in (Chatti et al., 2018a), a cubic volume with the size of 1 mm is a morphological RVE for a fibre volume fraction equal to 6%. As long as the fibre volume fraction is bigger than 6%, the conclusion is the same. For the three fibre volume fractions, f, tested: 6.5%, 8.5% and 10.5%, as seen in the previous paragraph, the relationship between the shear modulus and the distance between the cross-links is again a power law function with an exponent value of $-3/2$ (Fig. 11-a). In the considered range, the dependence of the shear stiffness, as a function of the distance between cross-links distance, does not seem to depend on the fibre volume fraction.

The fibre volume fraction is among the principle morphological parameters in a fibrous material. It can greatly influence the characteristics of an entangled cross-linked material. It does not influence only the mechanical properties but also thermic and acoustic properties. In this work, the influence of the fibre volume fraction on the shear stiffness was studied. Concerning the fibrous material, the relationship between the stiffness and the fibre volume fraction is considered as one of the most important properties in practical applications. The fibre volume fraction can be adjusted by changing the number of fibres introduced in the box of the RVE for FE simulations.

The technique to generate the cross-links illustrated in Fig. 9 does not allow the fixation of the average distance between cross-links. This value is computed in each case and depends on fibre volume fraction, on fibre diameter and on the proportion of. So, three average distances between cross-links were taken from the curve plotted in Fig. 11-a ($D_c = 150\,\mu$m, $D_c = 205\,\mu$m, $D_c = 260\,\mu$m). For each average distance between the cross-links, the effect of the fibre volume fraction on the shear modulus is shown as a function of fibre volume fraction (Fig. 11-b). The finite element simulation results indicate that the shear modulus is a linear function of the fibre volume fraction of the entangled cross-linked fibrous material. This result is consistent with Eq. (2) that provides the shear modulus proposed by Cox (1952). It agrees also with the stiffness study of Markaki and Clyne (2005). The slopes of the three curves in Fig. 11-b are different because they depend on the average distance between cross-links. The slope of each curve increased with the decrease of the average distance between cross-links. Thus, the fibre volume fraction impacted the shear stiffness more for the small average distance between cross-links (Table 2). The increase of the fibre volume fraction slightly impacted the

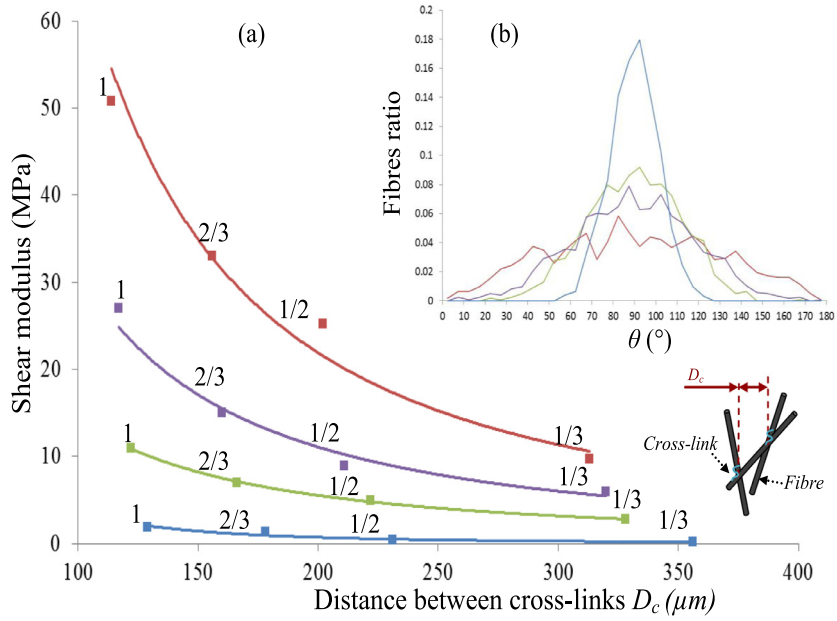

Fig. 10. (a) Influence of the average distance between cross-links on shear modulus for (b) different distributions of fibre orientations and different proportion of bonded contacts (one-third, one-half, two-thirds and one).

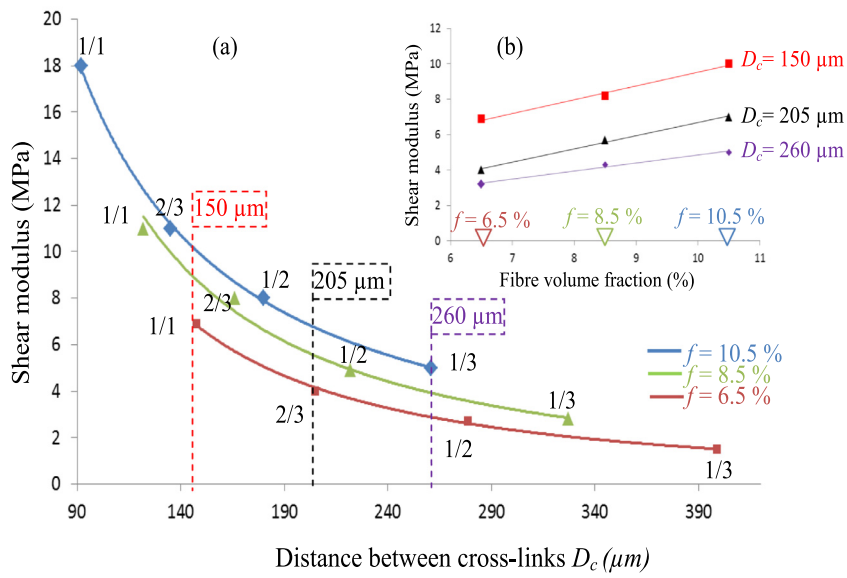

Fig. 11. Influence of fibre volume fraction and distance between cross-links on the shear stiffness.

Table 2
Values of slope for different average distance between cross-links: $D_c = 150\,\mu m$, $D_c = 205\,\mu m$ and $D_c = 260\,\mu m$.

Average distance between cross-links D_c (μm)	Value of slope(MPa/%)
150	0.77
205	0.75
260	0.45

Table 3
Young's modulus of different fibre nature: carbon, Inox, glass and aramid.

Nature	Young's modulus E (GPa)
Carbon	240
Stainless steel	180
Glass	73
Aramid	36

shear modulus. Nevertheless, it should be chosen carefully so it does not impact the good ratio weight/stiffness of material.

3.2.3. Effect of nature of fibre on the shear modulus for different distributions of fibre orientations

An entangled cross-liked material can be manufactured by different types of fibres, such as carbon, stainless steel, aramid or glass. The actual numerical model can provide a good idea about the effect of the fibre type by comparing four different materials. The study of the effect of the fibre type is always done for the no-perfect separated fibres case ($D_h = \sqrt{2}D$). The Young's modulus for each kind of fibre is presented in Table 3. To respect the approach of homogenization, half of the Young's modulus was intro-

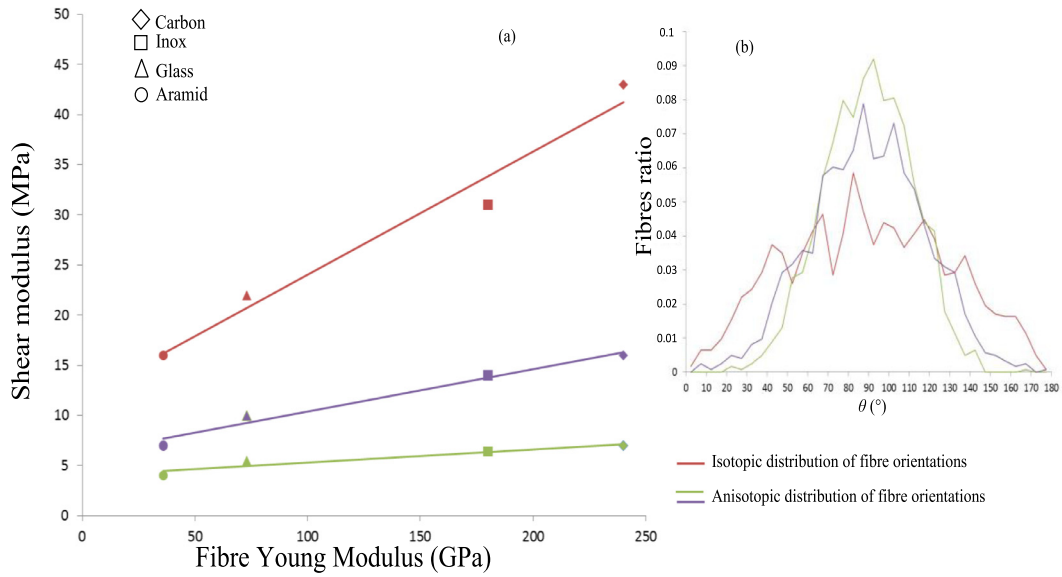

Fig. 12. The effect of Young's modulus corresponding to different types of fibre (carbon, Inox, glass and aramid) on the shear stiffness of the RVE for a fibre volume fraction of 8.5%; three distributions of fibre orientations were studied (one isotropic and two anisotropic).

Table 4
Values of the slope for three different distributions of fibre orientations presented in Fig. 12-b.

Distribution of fibre orientations		Value of slope (%)
Anisotropic distribution	Green curve (Fig. 12-b)	1.3
	Purple curve (Fig. 12-b)	4.2
Isotropic distribution		12

duced numerically in the model for each case. The volume fraction was equal to 8.5% for each case and the same joint stiffness was used, namely 0.4 N/mm for the spring tension stiffness, K_{te}, and 3.10^{-4} N.mm for the joint twisting stiffness, K_{tw}. 2/3 of contacts between fibres were bonded by 6000 springs. Thus, the average distance between the cross-links was around 160 µm for all RVE made with the three different types of fibre.

The effect of the type of fibre on the shear modulus for an entangled cross-linked fibrous material can be evaluated from the relationship between the shear modulus and the Young's modulus of the fibre. The influence of the type of fibre on the shear modulus was tested for different distributions of fibre orientations (Fig. 12-b). In each one, the shear stiffness increased with the increase of the fibre Young's modulus. The relationship between the shear stiffness and the Young's modulus was a linear function, which agrees with the literature studying the stiffness of a fibrous material (Cox, 1952; Gibson and Ashby, 1997b; Markaki and Clyne, 2005).

The slope of the curve corresponding to the isotropic distribution of fibre orientations is the biggest, with a value of 12%. The value of the slope decreased when there were more fibres with horizontal direction (anisotropic distribution), as illustrated in Table 4. The intrinsic stiffness of the fibres seems to have a more pronounced effect on the shear modulus for an isotropic distribution of fibre orientations. As the anisotropy of the distribution increases (increase of the proportion of fibre between 45° and 135°), the shear modulus decreases but the effect of the intrinsic stiffness of the material also seems to decrease.

3.2.4. *Effect of joint tension stiffness on the shear modulus*

In this section, the influence of the spring tension stiffness on the shear modulus for different distances between the cross-links was studied (Fig. 13). The other morphological parameters were fixed. The initial fibre volume fraction was equal to 8.5%, two-thirds of the contacts were bonded by epoxy junctions and the distribution of fibre orientations was as shown in Fig. 2 (green curve). The twisting stiffness was equal to 3.10^{-4} N.mm.

For all tested geometries, the shear stiffness of the fibrous material increased with the value of the joint tension stiffness (Fig. 13). The shear stiffness of material can be significantly increased by using a higher rigidity resin. The relationship between the shear modulus and the joint tension stiffness is well fitted by logarithmic function, as illustrated in Fig 13. However, the change of the resin also caused a modification in the viscosity, and the average distance between the junctions in the real material and these effects on the manufacturing process, cannot be modelled here but must be kept in mind.

The effect of the spring stiffness for different distances between the junctions is shown in Fig. 13. Firstly, as expected, when the average distance between junctions, D_c, is shorter, then the shear stiffness of the material is higher. Secondly, the more the distance between junctions decreases, the more the material stiffness can increase when the joint tension stiffness increases, as shown in Fig. 13 (curves I and II). The displacement of the fibres in this case was mainly due to the bending displacement of the beam. When the distance between the junctions decreased, the stiffness was mainly due to the spring stiffness, which indicated that the spring had a greater influence.

3.2.5. *Effect of joint twisting stiffness on the shear modulus*

In Fig. 14, the twisting stiffness of the joint was varied to study the influence of this parameter on the shear behaviour. The other morphological parameters were fixed. The initial fibre volume fraction was equal to 8.5%, the distribution of fibre orientations is as presented in Fig. 2 and the tension stiffness was equal to 0.4 N/mm. Three different values for the distance between the cross-links were studied. The shear modulus increased slightly with the increase of the spring twisting stiffness, and it became stable starting with K_{tw} equal to 0.0015 N.mm. There was not a clear effect of the twisting stiffness on the shear modulus for

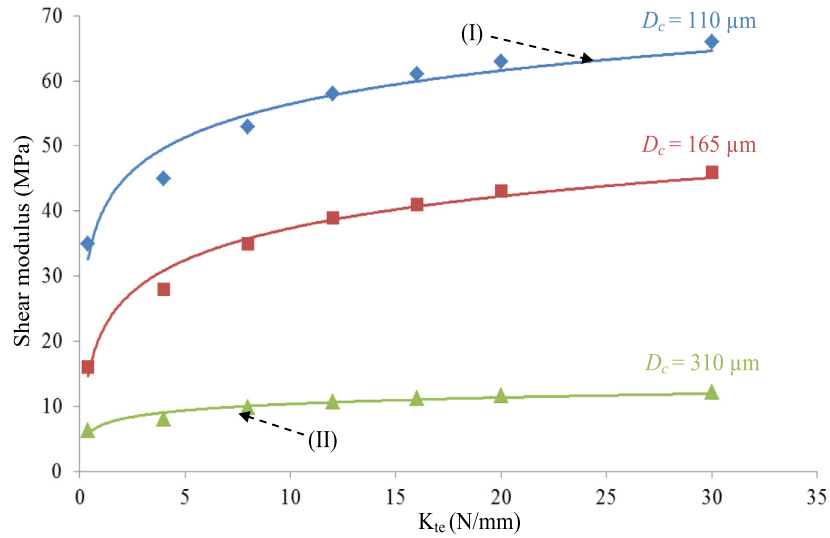

Fig. 13. Influence of joint tension stiffness on shear modulus for different distances between cross-links. All tested RVE had the same configuration and a fibre volume fraction equal to 8.5%. The values of $D_c = 110\,\mu m$, $D_c = 165\,\mu m$ and $D_c = 310\,\mu m$ correspond to the bonding of all contacts, 2/3 of contacts and 1/3 of contacts, respectively.

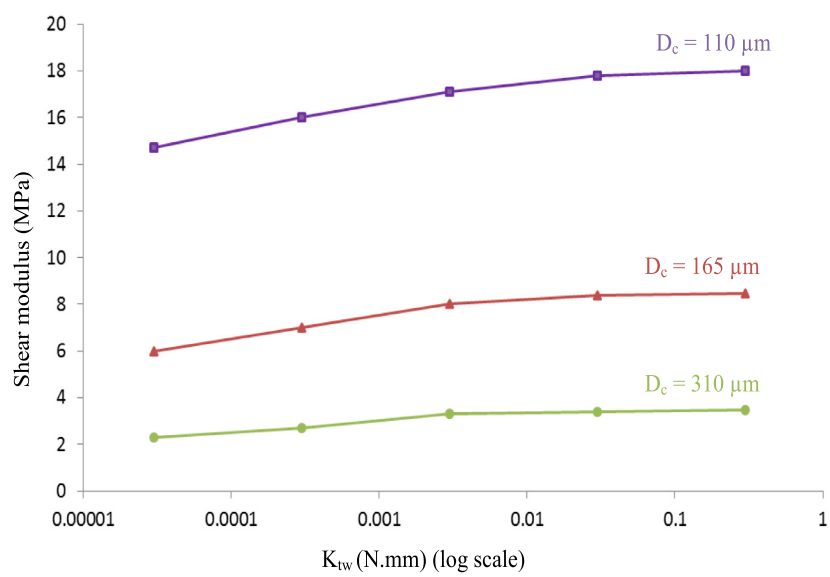

Fig. 14. Influence of joint twisting stiffness on shear modulus for different distances between cross-links. The same configuration is used for all tested RVE with a fibre volume fraction equal to 8.5%. The $D_c = 110\,\mu m$ corresponds to all bonded contacts, $D_c = 165\,\mu m$ to 2/3 of the bonded contacts and $D_c = 310\,\mu m$ to 1/3 of the bonded contacts.

different distances between the cross-links. Even if the twisting stiffness, K_{tw}, was increased significantly (log scale of the curve), there was not a clear change on the shear modulus. It was neglected compared to the influence of the tension stiffness. This result shows that the junctions were more solicited in tension than in twisting.

4. Conclusions

The main objective of the current work was to study the stiffness in shear of the entangled cross-linked fibrous material. The numerical model focused on the influence of the morphological parameters on the shear behaviour of the entangled cross-linked material. This investigation was an interesting tool to understand the behaviour of entangled cross-linked materials in order to optimize it and enhance their mechanical properties. The work represents a robust base for developing a manufacturing process that can offer an entangled cross-linked material with the best of its stiffness rigidity.

A finite element model was developed to predict the stiffness of an entangled cross-linked material in shear. It used 3D beam elements to simulate all modes of fibre deformation. The comparison between the numerical results and the experimental data showed a good agreement in terms of shear modulus when an assumption concerning non-separated yarns was considered. Then, a numerical investigation was carried out to study the effect of morphological parameters on the shear stiffness. The obtained results showed that the perfect separation of yarns during manufacturing process can improve the mechanical properties of the fibrous material.

The relationship between the shear modulus and the average distance between cross-links was fitted by a power law function with an exponent of −3/2. The increase of the number of epoxy cross-links, which causes the decrease of the average distance between junctions, can allow the increase of the rigidity of our fibrous material. This can be done by spraying more resin, but in

this case, the density of the sample will increase and the ratio stiffness/mass will then decrease. Process improvements, in order to have a more efficient bonding of the junctions, are to be studied. The question is: how to have the finest droplets condensing on all the contact points while minimizing the presence of resin elsewhere? The creation of a greater number of junctions requires a spraying of very fine drops of resin of good fluidity. An improvement in the actual manufacturing process, and in particular, the process of entanglement and spraying of the resin, could thus generate significant gains in the actual rigidity of our entangled cross-linked material.

The relationship between the shear modulus and the fibre volume fraction or the Young's modulus is a linear function. This result is in good agreement with the former studies. It confirms that these two parameters have a first-rate effect on the rigidity of these types of fibrous material. Due to their high specific rigidity, high modulus carbon fibres are the ideal candidates for this application. The increase of the tension joint stiffness can increase the shear modulus, but the twisting joint stiffness did not have an important effect on the shear stiffness of the entangled cross-linked fibrous material. The increase of the rigidity of the junctions can be obtained experimentally through the modification of the mechanical properties of the resin and / or the increase of the size of the sprayed resin droplets. The latter is quite delicate to control during the phase of spray. Surface treatments of the fibres could modify the surface energy of the fibres and thus modify the size and morphology of the junctions.

It is also important to remember that in a targeted application of sandwich panel core materials, the properties of the complete sandwich must be studied and modelled for both static and vibratory loads, for which the damping potential of the interlocking materials is very interesting.

The management of morphological parameters can improve the shear stiffness of entangled cross-linked fibrous material such that a good value of the shear modulus can be reached that is comparable to that of Nomex honeycombs and PMI foam. Nevertheless, these morphological parameters should be carefully chosen to enhance the mechanical properties of the entangled cross-linked material without impacting its good vibration damping properties (Piollet et al., 2016; Chatti et al., 2018). This improvement will make the entangled cross-linked fibrous material relevant for use in structural applications as a core material for vibration damping.

Acknowledgements

Thanks are due to CALMIP under the reference of program P1026 for the support and the computing power. Financial support for this work was obtained thanks to the joint project MAFIVA funded by the Midi-Pyrénées region and by ISAE-SUPAERO.

References

Ashby, M.F., Evans, A.G., Fleck, N.A., Gibson, L.J., Hutchinson, J.W., 2000. Wadley HNG. Metal foams: A Design Guide. Butterworth- Heinemann, Boston.

Belouettar, S., Abbadi, A., Azari, Z., Belouettar, R., Freres, P., 2009. Experimental investigation of static and fatigue behaviour of composites honeycomb materials using four point bending tests. Compos. Struct. 87, 265–273.

Cai, C., Zheng, H., Liu, G., 2004. Vibration analysis of a beam with PCLD patch. Appl. Acoust. 65, 1057–1076.

Castanié, B., Aminanda, Y., Bouvet, C., Barrau, JJ., 2008. Core crush criterion to determine the strength of sandwich composite structures subjected to compression after impact. Compos. Struct. 243–250.

Chatti, F., Bouvet, C., Poquillon, D., Michon, G. , 2018a. Numerical modelling of shear hysteresis of entangled cross-linked carbon fibres intended for core material. Comput. Mater. Sci. 155, 350–363.

Chatti, F., Poquillon, D., Bouvet, C., Michon, G. , 2018b. Numerical modelling of entangled carbon fibre material under compression. Comput. Mater. Sci. 151, 14–24.

Cox, H.L., 1952. The elasticity and strength of paper and other fibrous materials. Br. J. Appl. Phys. 3, 72–79.

Delannay, F., 2005. Elastic model of an entangled network of interconnected fibres accounting for negative Poisson ratio behaviour and random triangulation. Int. J. Solids Struct. 42, 2265–2285.

Delince, M., Delannay, F., 2004. Elastic anisotropy of a transversely isotropic random network of interconnected fibres: non-triangulated network model. Acta Mater. 52, 1013–1022.

Fotsing, E., Sola, M., Ross, A., Ruiz, E., 2013. Lightweight damping of composite sandwich beams: experimental analysis. J. Compos. Mater. 47, 1501–1511.

Gibson, L.J., Ashby, M.F., 1997a. Cellular Solids: Structure and Properties. Cambridge University Press.

Gibson, L.J., Ashby, M.F., 1997b. Cellular Solids Structure and Properties., 2nd ed Cambridge University Press.

Heyden, S., 2000. Network Modelling for the Evaluation of Mechanical Properties of Cellulose Fibre Fluff. Lund University, Sweden Ph.D. thesis.

J.A. Van den Akker, Some theoretical considerations on the mechanical properties of fibrous structures. In: Trans. Brit. Paper and Board Makers' Assoc. Sympos. Consol. Paper Web, (1962) pp. 205–241, London.

Jin, M.Z., Chen, C.Q., Lu, T.J., 2013. The mechanical behavior of porous metal fiber sintered sheets. J. Mech. Phys. Solids 61, 161–174.

Kallmes, O.J., Corte, H., 1960. The structure of paper, I. The statistical geometry of an ideal two dimensional fibre network. Tappi 43, 737–752.

Kallmes, O.J., Stockel, I.H., Bernier, G.A., 1963. The elastic behaviour of paper. Pulp Pap. Mag. Can. 64 (10), T449–T456.

Kanit, T., Forest, S., Galliet, I., Mounoury, V., Jeulin, D., Determination of the size of the representative volume element for random composites: statistical and numerical approach, Int. J. Solids Struct. (2003) Vol. 40(13–14), pp 3647–3679

Komori, T., Makishima, K., 1977. Number of fiber-to-fiber contacts in general fiber assemblies. Text. Res. J. 47 (13), 13–17.

Li, Z., 2006. Vibration and acoustical properties of sandwich composite materials. Thèse De Doctorat. Auburn University.

Ma, Y.H., Zhu, H.X., Su, B., Hu, G.K., Perks, R., 2018. The elasto-plastic behavior of three-dimensional stochastic fibre networks with cross-linkers. J. Mech. Phys. Solids 110, 155–172.

Markaki, A.E., Clyne, T.W., 2005. Magneto-mechanical actuation of bonded ferromagnetic fibre arrays. Acta Mater. 53, 877–889.

Mezeix, L., Bouvet, C., Huez, J., Poquillon, D., 2009. Mechanical behaviour of entangled fibers and entangled cross-linked fibers during compression. J. Mater. Sci. 44 (14), 3652–3661.

Mezeix, L., Poquillon, D., Bouvet, C. , 2015a. Entangled cross-linked fibers for an application as core material for sandwich structures part I: experimental investigation. Appl. Compos. Mater. 23 (1), 71–86.

Mezeix, L., Poquillon, D., Bouvet, C. , 2015b. Entangled cross-linked fibres for an application as core material for sandwich structures – part II: analytical model. Appl. Compos. Mater. 1–14.

Piollet, E., Poquillon, D., Michon, G., 2016. Dynamic hysteresis modelling of entangled cross-linked fibres in shear. J. Sound Vibr. 383, 248–264.

Poquillon, D., Viguier, B., Andrieu, E., 2005. Experimental data about mechanical behaviour during compression tests for various matted fibres. J. Mater. Sci. 40, 5963–5970.

Silva, M.J., Gibson, L.J., 1997. The effects of non-periodic microstructure and defects on the compressive strength of two-dimensional cellular solids. Int. J. Mech. Sci. 39, 549–563.

User Documentation, ABAQUS user's manual: version 6.11.

van Wyk, C.M., 1946. Note on the compressibility of wool. Text. Res. J. Inst. 37, T285–T292.

Zenkert, D., 1997. The Handbook of Sandwich Construction. Eds Engineering Materials Advisory Services Ltd.